



UNIVERSITY OF LEEDS

This is a repository copy of *Strategy for preventing excessive wear rate at high loads in bulk metallic glass composites*.

White Rose Research Online URL for this paper:
<http://eprints.whiterose.ac.uk/121507/>

Version: Accepted Version

Article:

Villapún, VM, Medina, J, Pérez, P et al. (3 more authors) (2017) Strategy for preventing excessive wear rate at high loads in bulk metallic glass composites. *Materials & Design*, 135. pp. 300-308. ISSN 0261-3069

<https://doi.org/10.1016/j.matdes.2017.09.035>

© 2017 Elsevier Ltd. This manuscript version is made available under the CC-BY-NC-ND 4.0 license <http://creativecommons.org/licenses/by-nc-nd/4.0/>

Reuse

Items deposited in White Rose Research Online are protected by copyright, with all rights reserved unless indicated otherwise. They may be downloaded and/or printed for private study, or other acts as permitted by national copyright laws. The publisher or other rights holders may allow further reproduction and re-use of the full text version. This is indicated by the licence information on the White Rose Research Online record for the item.

Takedown

If you consider content in White Rose Research Online to be in breach of UK law, please notify us by emailing eprints@whiterose.ac.uk including the URL of the record and the reason for the withdrawal request.

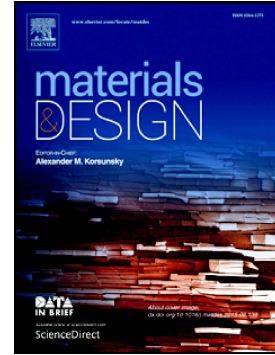


eprints@whiterose.ac.uk
<https://eprints.whiterose.ac.uk/>

Accepted Manuscript

Strategy for preventing excessive wear rate at high loads in bulk metallic glass composites

Victor M. Villapún, J. Medina, P. Pérez, F. Esat, F. Inam, S. González



PII: S0264-1275(17)30880-8
DOI: doi: [10.1016/j.matdes.2017.09.035](https://doi.org/10.1016/j.matdes.2017.09.035)
Reference: JMADE 3368

To appear in: *Materials & Design*

Received date: 28 June 2017
Revised date: 16 September 2017
Accepted date: 18 September 2017

Please cite this article as: Victor M. Villapún, J. Medina, P. Pérez, F. Esat, F. Inam, S. González, Strategy for preventing excessive wear rate at high loads in bulk metallic glass composites, *Materials & Design* (2017), doi: [10.1016/j.matdes.2017.09.035](https://doi.org/10.1016/j.matdes.2017.09.035)

This is a PDF file of an unedited manuscript that has been accepted for publication. As a service to our customers we are providing this early version of the manuscript. The manuscript will undergo copyediting, typesetting, and review of the resulting proof before it is published in its final form. Please note that during the production process errors may be discovered which could affect the content, and all legal disclaimers that apply to the journal pertain.

Strategy for preventing excessive wear rate at high loads in bulk metallic glass composites

Victor M. Villapún^a, J. Medina^b, P. Pérez^b, F. Esat^c, F. Inam^a, S. González^a

^aFaculty of Engineering and Environment, Northumbria University, Newcastle upon Tyne NE1 8ST, UK

^bCentro Nacional de Investigaciones Metalúrgicas, CSIC, Avda. Gregorio del Amo 8, 28040 Madrid, Spain

^cSchool of Chemical and Process Engineering, University of Leeds, Leeds LS2 9JT, UK

Keywords: Tribological properties; Doping element; Metallic glass composite; Pin-on-disc

*Corresponding author. Tel.: +44 (0) 191 349 5937

E-mail address: sergio.sanchez@northumbria.ac.uk (S. González)

Abstract

The effect of nickel additions to tune the wear performance of $\text{Cu}_{45.5}\text{Zr}_{51}\text{Al}_{3.5}$ at. % alloy has been studied to present a new strategy for preventing excessive wear rate at high loads in metallic glass composites. This strategy consists on proper selection of a doping element in controlled concentrations with the ability to decrease the glass transition temperature (T_g) of the alloy so that the friction temperature during sliding is close to the T_g . This enables the formation of crystalline phases and their subsequent oxidation (lubricating layer) on the contact surface during sliding thus enhancing the wear resistance. Proper doping can also contribute towards the wear resistance when the content of the doping element promotes the martensitic transformation. The results show that the main wear mechanism for the three studied alloys ($\text{Cu}_{45.5}\text{Zr}_{51}\text{Al}_{3.5}$, $\text{Cu}_{44.5}\text{Zr}_{51}\text{Al}_{3.5}\text{Ni}_1$ and $\text{Cu}_{43.5}\text{Zr}_{51}\text{Al}_{3.5}\text{Ni}_2$ at. %) is governed by delamination and the mass loss increases with increasing load from 1 to 10 N. However, for the maximum load of 15 N, the calculated friction temperature is close to T_g for the Ni-containing alloys and partial crystallization and oxidation take place resulting in a mass loss decrease from about 2.6 mg (at 10 N) to about 2.1 mg (at 15 N).

1. Introduction

Bulk metallic glasses (BMGs) are interesting materials due to their unique chemical and physical properties. Due to the combination of high hardness and high strength metallic glasses are expected to exhibit superior wear resistance and therefore they are promising materials for tribological applications. Higher values of the wear resistance were reported when BMGs are annealed [1] or when proper volume fractions of crystalline phases are embedded in the amorphous matrix (i.e., BMG composites) [2] for multiple alloy systems such as Fe-based [3], Zr-based [4] and Cu-based alloys [5]. The wear resistance can also be increased when a dissimilar/oxide layer is formed on the sliding interface of Ti-based [6], Zr-based BMGs [7] and on metal surfaces in general [8].

Previous studies suggest that during dry sliding, surface oxidation can occur when the contact temperature is near the glass transition temperature (T_g) [7] and above T_g [9] due to the high oxygen permeability of the oxide film formed in the supercooled liquid region where the viscosity drops. Additionally, the lack of long-range order inherent to amorphous materials can lead to microstructural changes during contact sliding, changing the wear performance of the material [10, 11]. In this regard, contact temperature plays a central role in the wear performance of metallic glasses [11, 12]. Insufficient temperature to promote crystallization can lead to super-plasticity and softening of the material, increasing the wear rate of the BMG [13] but when the temperature is high enough to result in microstructural changes, the wear rate decreases [14].

The wear rate not only depends on the volume fraction of crystalline phases embedded in the amorphous matrix [2] but also on their nature. Among these crystalline phases, shape memory phases are of interest since they exhibit stress induced martensitic transformation. Erosion resistance of martensite is superior to that of austenite [15], which can explain the interest in promoting the formation of martensite. An efficient method to do that is doping (i.e., microalloying) using elements such as Fe, Co and Ni because when added in the proper concentrations they can decrease the stress for transformation of CuZr austenite into CuZr martensite [16, 17]. As a result, BMG composites with CuZr martensite phase embedded in the amorphous matrix are of interest to enhance the wear resistance.

The aim of this study is to propose a new strategy to decrease the wear rate of BMG composites at high loads based on controlled doping to promote partial surface crystallization and oxidation while at the same time promoting martensitic transformation of the crystalline phase. This strategy is expected to have important implication in the design of Micro-Electro-Mechanical Systems (MEMS) such as microgears and microbearings, where wear resistance enhancement is primordial to extend their service life [18, 19]. We have shown that the friction temperature (ΔT_{max}) can be estimated from the equation given by Wu et al. [20] and that it gives sensible values to compare with the glass transition temperature of the doped alloy to be able to estimate whether the alloy will exhibit massive wear ($\Delta T_{max} \ll T_g$) or decreased wear ($\Delta T_{max} \geq T_g$).

2. Experimental

Alloy ingots of nominal composition $\text{Cu}_{45.5}\text{Zr}_{51}\text{Al}_{3.5}$, $\text{Cu}_{44.5}\text{Zr}_{51}\text{Al}_{3.5}\text{Ni}_1$ and $\text{Cu}_{43.5}\text{Zr}_{51}\text{Al}_{3.5}\text{Ni}_2$ (at. %) were prepared from elements with purity higher than 99.9 at. %. The master alloys were re-melted three times in a Ti-gettered high purity argon atmosphere to attain good chemical homogeneity. Rod samples of 2 mm in diameter were obtained from the master alloy by copper mould casting in an inert gas atmosphere. The structure of the as-cast samples was studied by X-ray diffraction (XRD) using a Bruker D8 diffractometer with monochromated $\text{Cu K}\alpha$ radiation (2 θ range 20°-90°, step size = 0.03°). Thermal behaviour of the samples were studied using differential scanning calorimetry (DSC, SETARAM C131 EVO) at a constant heating rate of 20 K/min up to 773 K. The microstructure was investigated by scanning and transmission electron microscopy (SEM and TEM respectively). Dry sliding wear experiments were conducted using a pin-on-disc (DUCOM Micro POD) in dry conditions in air at room temperature following the ASTM-G99. The pins were made from BMG composite rods and the counterbody disc was En 31 steel hardened to 60 HRC and ground to 1.6 μm (Ra) surface roughness. Tests were performed at increasingly loads of 1, 5, 10 and 15 N at a sliding velocity of 0.5 m/s for a sliding distance of 1800 m. Mass loss was obtained by measuring the weight of the pins after and before the tests by using an analytical balance (Acculab Sartorius group, $\pm 0.1\text{mg}$).

3. Results and discussion

3.1. Microstructure of the as-fabricated pins

Figure 1 shows the XRD patterns for the three compositions selected in this study. For the $\text{Cu}_{45.5}\text{Zr}_{51}\text{Al}_{3.5}$ alloy (Fig. 1a), the scan shows the presence of peaks that could be associated with orthorhombic $\text{Cu}_{10}\text{Zr}_7$ ($a = 0.9347\text{ nm}$, $b = 0.9347\text{ nm}$, $c = 1.2675\text{ nm}$), orthorhombic Cu_8Zr_3 ($a = 0.78686\text{ nm}$, $b = 0.81467\text{ nm}$, $c = 0.9977\text{ nm}$), austenite B2 CuZr ($a = 3.2562\text{ nm}$, $b = 3.2562\text{ nm}$, $c = 3.2562\text{ nm}$), monoclinic martensite B19' CuZr ($a = 0.3237\text{ nm}$, $b = 0.4138\text{ nm}$, $c = 0.5449\text{ nm}$) and tetragonal CuZr_2 ($a = 0.3220\text{ nm}$, $b = 0.3220\text{ nm}$, $c = 1.1183\text{ nm}$). These peaks are superimposed on a broad halo, suggesting the presence of an amorphous matrix. For the $\text{Cu}_{44.5}\text{Zr}_{51}\text{Al}_{3.5}\text{Ni}_1$ alloy (Fig. 1b), the scan is very similar but an additional small peak at 56.5° is observed, which could be attributed to CuZr martensite. For the alloy with 2 at. % Ni content (Fig. 1c), the main peak detected at 39.3°, corresponding to $\text{Cu}_{10}\text{Zr}_7$, Cu_8Zr_3 and CuZr_2 , decreases in intensity while for the peak at 29.7°, attributed to Cu_8Zr_3 , increases. These results suggest that there is no clear trend in the evolution of the glass forming ability (GFA) with the composition change.

The thermal behaviour of the three compositions was studied by running DSC scans at 20 K/min up to 765 K (Fig. 2). The glass transition temperature (T_g), crystallization onset temperature (T_x), super-cooled liquid region (ΔT) and crystallization enthalpy (H) have been measured and

listed on Table 1. The T_g was evaluated from the tangent crosspoint while the crystallization enthalpy (ΔH) was obtained by integrating the area under the exothermic peak. For $\text{Cu}_{45.5}\text{Zr}_{51}\text{Al}_{3.5}$ alloy $T_g = 710.84$ K and $H = 47.05$ J/g while a small addition of Ni to 1 at. % lowers the T_g to 697.77 K and H to 49.08 J/g. Further addition of Ni to 2 at. % decreases the T_g to 685.39 K and the enthalpy decreases slightly to 42.54 J/g. The decrease of T_g would suggest that the amorphous structure becomes destabilized with increasing Ni content, which could be attributed to the positive heat of mixing with Cu (Ni-Cu: +4 kJ/mol). On the other hand, the heat of mixing of Cu-Zr is negative (-23 kJ/mol) [21] and therefore increasing Ni addition, which has unfavourable mixing relationships with Cu, would promote the formation of intermetallic Cu-Zr phases, which agrees with higher intensity of the XRD peak for Cu_8Zr_3 detected at about 30° (Fig. 1).

The results show that the increase in nickel content shifts the glass transition temperature towards smaller values (inset of Fig. 2) and this has an effect on the crystallization process, as deduced from the increase in heat flow values and narrowing of the transformation peaks. However, increasing Ni additions does not have an important effect on the evolution of the ΔH and therefore neither on the GFA of the alloys, which is in good agreement with XRD results (Fig. 2). This suggests that the parameter ΔT_x is not a good GFA indicator for these compositions [22]. The crystallization onset temperature (T_x) has been measured from the tangent crosspoint. The crystallization temperature is maximum for the $\text{Cu}_{45.5}\text{Zr}_{51}\text{Al}_{3.5}$ alloy (744.87 K) and decreases with addition of 1 at. % Ni to 740.57 K, while no significant changes were observed for further addition to 2 at. % (740.06 K). The calculated supercooled liquid region ($\Delta T_x = T_x - T_g$) tends to increase with increasing Ni content from 0 to 2 at. % (34.03 K, 42.80 K and 54.66 K) and these results are consistent with the values reported in the literature for similar compositions [23].

3.2. Wear tests

3.2.1. Friction coefficient and wear rate

The mechanical behaviour of the $\text{Cu}_{45.5}\text{Zr}_{51}\text{Al}_{3.5}$, $\text{Cu}_{44.5}\text{Zr}_{51}\text{Al}_{3.5}\text{Ni}_1$ and $\text{Cu}_{43.5}\text{Zr}_{51}\text{Al}_{3.5}\text{Ni}_2$ (at. %) alloys were studied from dry sliding wear tests using a pin-on-disc at different loads (1, 5, 10 and 15 N). For simplicity, tested samples have been coded according to the composition and load applied as listed in Table 2. The evolution of the wear behaviour has been obtained by measuring the friction coefficient (COF) and mass loss for all the studied pins for different compositions and loads as presented in Fig. 3a and Fig. 3b and measuring the evolution of the COF with the contact time (inset of Fig. 3a). The COF is a useful parameter to evaluate the wear behaviour since a small value indicates high wear resistance [24, 25]. The COF exhibits two stages (inset Fig. 3a) as commonly observed on wear tests, an initial rapid increase with time followed by a steady-state stage [24]. For the Ni-containing alloys (Ni1 and Ni2) the COF is approximately constant at low loads and increases dramatically for loads higher than 5 N. The curve for the alloy without Ni (i.e., $\text{Cu}_{45.5}\text{Zr}_{51}\text{Al}_{3.5}$) shows a similar evolution with increasing load but exhibits a slight shift to the right of about 5 N. For this last alloy the COF is approximately constant, about 0.6, for up to 10 N (1NNi0,

5NNi0 and 10NNi0) and therefore it is close to the range of values of 0.4 to 0.6 obtained by Rahamand et al. [13] for a Cu-Zr-Al system with Cu/Zr \approx 1 and similar loading conditions. In contrast, when the load reaches 15 N the COF is about 0.9 while for the Ni-containing alloys it is about 1. The increase in the COF for high loads is consistent with that observed by Bhatt et al. [26] for a Cu-based BMG, which was attributed to the increase in debris formation due to the brittle fracture of crystallized BMG. In order to investigate this, the microstructures have been analysed (see section 3.2.2. SEM and TEM analysis).

Figure 3b shows the mass loss for the studied alloys subjected to different loads (1, 5, 10 and 15 N) after sliding for 1 h. The mass loss for 1 N is practically the same for all the compositions (i.e., 0.25), however, the mass loss at higher loads is different for each composition. The mass loss for the alloy without Ni increases with increasing load and reaches a maximum value of about 3.8 mg for 15 N. However, for the alloys with 1 and 2 at. % Ni, the evolution of the mass loss with increasing load is similar between them and different from the alloy without nickel. For both compositions the mass loss increases with increasing load to a maximum of about 2.7 mg for 10 N and decrease to about 2.1 mg for 15 N. In order to explain this behaviour, the microstructure has been studied in detail in section 3.2.2. (SEM and TEM analysis). The worn surface of the pins after the test is shown in the secondary electron SEM images of Fig. 4. The surface of these samples consists of long continuous grooves a few micrometers in width induced by ploughing (see insets), which is a common feature of abrasive wear [13]. This grooved surface can be also noticed for 5 N and 10 N conditions with the progressive disappearance of this feature due to increasing delamination of the sample with the load thus suggesting a change in the wear mechanism with increasing load [27]. Maximum delamination is observed for the samples tested at 15 N (see insets) for which patches of smeared material (areas of dark tonality on the images) partly covering the grooves are also present.

Delamination is normally considered as the main wear mechanism of metallic glasses [27] and it is generated by shear forces acting on the material upon sliding. For high enough load, the surface layer deforms plastically and subsurface cracks nucleate and propagate resulting in the formation of loose wear sheets (i.e., delamination) [28]. Overall, the surfaces of the 1 N and 5 N samples are mostly clean without signs of cracks and delamination, which can explain the constant COF values of about 0.6. On the other hand, the samples subjected to 10 N and 15 N load exhibit small fractures or microcracks attributed to highly localized shear forces (red circles and white arrows in Fig. 4) more noticeable as the load increases. Yang et al. [29] demonstrated that these cracks are the result of nucleation and propagation of surface and subsurface cracks leading to delamination (i.e., flakes), which is in agreement with the enhanced tendency for delamination and microcracking view in the samples tested at the highest load. Small differences in delamination can be appreciated between the 10NNi1 and 10NNi2 samples and the 10NNi0 alloy. Ni-containing alloys show more delamination than the Ni-free alloy, accounting for their higher loss mass of the Ni content alloys. The presence of long cracks and delamination is especially noticeable for the 15NNi0 sample, indicating that the high mass loss displayed by this sample would be caused by the

increase in delamination.

A common feature for all samples is the presence of small debris particles distributed on the worn surfaces of the pins whose density tends to increase as the load increases. This debris can be attributed to the formation of Zr oxides as shown by Hong et al. [30] due to the temperature rise during friction. Additionally, patches of smeared material can be noticed for loads higher than 1 N. The presence of smeared material in similar amounts for the three compositions but in increasing volume fraction as the load increases suggest that these patches are more related to changes in the loading conditions than compositional differences. The hard intermetallic particles released from the pin due to friction forces can remove material from the soft steel disc during dry sliding and attach to the pin [31].

In order to investigate the particles and patches present on the worn surfaces in more detail, these features have been observed at higher magnification and the composition has been analysed. Considering that these features do not depend on the composition of the alloy and for the sake of simplicity, only the alloys without nickel have been studied. Figure 5 shows the magnified backscattered SEM images of the worn surfaces for 1NNi0 (Fig. 5a) and 15NNi0 (Fig. 5b) after the wear test. For 1NNi0 small particles of dark tonality homogeneously distributed are observed. EDX microanalysis of these particles (such as the one shown inside the red circle in Fig. 5a) indicate that they are rich in oxygen (47.6 at. % O, 26.3 at. % Cu, 23.9 at. % Zr 2.3 at. % Al) and therefore they could correspond to an oxide, which is consistent with the dark tonality. For 15 N, dark patches from a few microns up to more than 100 μm long are oriented along the groove direction. The composition of these patches (see red rectangle for the area analysed in Fig. 5b) is 50.7 at. % O, 19.4 at. % Fe 14.6 at. % Cu, 13.7 at. % Zr 1.3 at. % Al, 0.4 at. % Cr. The high oxygen content and presence of Fe and Cr confirms that part of the debris originates from the stainless steel disc that undergoes oxidation due to the high friction temperatures reached. Inside the dark smeared patches, small clearer debris particles than the surrounded smeared material (white arrows) are also present but their composition could not be accurately discerned due to the small size.

3.2.2. Microstructural analysis after the tests

To understand the evolution in the wear performance of the samples, the microstructure of the pin surface after the pin-on-disc test have been analysed by SEM and TEM at the two extreme compositions and loads. Fig. 6 shows the secondary electron SEM images for $\text{Cu}_{45.5}\text{Zr}_{51}\text{Al}_{3.5}$ and $\text{Cu}_{43.5}\text{Zr}_{51}\text{Al}_{3.5}\text{Ni}_2$ samples at 1 and 15 N. For the 1NNi0 sample (Fig. 6a), particles with cubic and dendritic shape embedded in a featureless matrix can be observed. This matrix would correspond to the amorphous phase detected by XRD (Fig. 1a). The composition of the dendrites, according to the EDX analysis, ranges from $\text{Cu}_{42.2}\text{Zr}_{48.1}\text{Al}_{9.7}$ to $\text{Cu}_{43.01}\text{Zr}_{50.12}\text{Al}_{6.87}$ (Zr/Cu~1.15). The concentration in Zr is higher than that of the nominal composition (Zr/Cu~1.12) and considering that among the crystalline phases detected by XRD only CuZr_2 is richer in Zr than in Cu, the crystalline phase could correspond to CuZr_2 [32]. EDX analysis of the small black particles homogeneously distributed in

the matrix (white arrow in the inset of Fig. 6a) have a composition of $\text{Cu}_{52.7}\text{Zr}_{42.9}\text{Al}_{4.4}$ at. % ($\text{Zr}/\text{Cu}\sim 0.81$) and therefore might be attributed to $\text{Cu}_{10}\text{Zr}_7$.

When the sample is subjected to higher loads (15NNi0) the microstructure consists of dendrites surrounded by a globular halo (Fig. 6b). The dendrites (see inset) are of the same morphology and size (from 5 to $10\mu\text{m}$) as those observed for 1NNi0 and correspond to the same crystalline phase, i.e., CuZr_2 . The globular halo consists of two different crystalline phases (dark and clear tonality) of lamellar eutectic morphology. Considering that these are secondary electron images instead of backscattered images, the tonality does not give information about differences in atomic weight of the observed phases. From the composition of the darker phase, $\text{Cu}_{53.6}\text{Zr}_{43.0}\text{Al}_{3.7}$ ($\text{Zr}/\text{Cu}\sim 0.80$), and the clearer phase, $\text{Cu}_{50.4}\text{Zr}_{45.9}\text{Al}_{3.7}$ ($\text{Zr}/\text{Cu}\sim 0.91$), and considering the XRD scans (Fig. 1) it can be deduced that the phases may correspond to $\text{Cu}_{10}\text{Zr}_7$ and CuZr , respectively. The formation of the globular phase at 15 N may be caused by the increase in temperature due to the high friction force at the pin-disc contact. The formation of CuZr_2 dendrites, i.e., richer in Zr than the nominal composition, results in the formation of a surrounding area depleted in Zr and rich in Cu from where the crystalline phases $\text{Cu}_{10}\text{Zr}_7$ and CuZr can nucleate and grow.

Figure 6c shows that the microstructure for the 1NNi2 sample consists of small cubic and dendritic particles up to $5\mu\text{m}$ in size embedded in a featureless matrix. These particles are slightly more developed and the volume fraction is larger than for 1NNi0 sample. The composition of the cubic particles is $\text{Cu}_{38.4}\text{Zr}_{51.2}\text{Al}_{9.6}\text{Ni}_{0.8}$ ($\text{Zr}/\text{Cu}\sim 1.33$) while for the dendritic particles it is $\text{Cu}_{48.5}\text{Zr}_{46.4}\text{Al}_{2.8}\text{Ni}_{2.3}$ ($\text{Zr}/\text{Cu}=0.96$) and therefore can be associated with CuZr_2 and CuZr , respectively.

For the 15NNi2 sample (Fig. 6d), a dramatic change in microstructure can be seen. Large globular regions growing from the dendrites are observed and their morphology is similar to that observed for 15NNi0 (Fig. 6b), but they are so developed that some of them start to coalesce. The composition of the eutectic globular phases are $\text{Cu}_{46.2}\text{Zr}_{47.5}\text{Al}_{4.0}\text{Ni}_{2.3}$ and $\text{Cu}_{41.5}\text{Zr}_{52.6}\text{Al}_{3.5}\text{Ni}_{2.4}$ and may correspond to CuZr and CuZr_2 , respectively. These are stable phases of the ternary Cu-Zr-Al phase diagram [32-34], so their presence is indicative of an approach towards equilibrium conditions in the course of the wear tests. These two phases (CuZr_2 and CuZr) have also been observed by Cheng et. al. [35] for similar compositions $\text{Zr}_{50.1}\text{Cu}_{32.8}\text{Ni}_{9.1}\text{Al}_8$, $\text{Zr}_{52.8}\text{Cu}_{30.7}\text{Ni}_{8.5}\text{Al}_8$, $\text{Zr}_{55}\text{Cu}_{29}\text{Ni}_8\text{Al}_8$, $\text{Zr}_{57}\text{Cu}_{27.4}\text{Ni}_{7.6}\text{Al}_8$ and $\text{Zr}_{60}\text{Cu}_{25.1}\text{Ni}_{6.9}\text{Al}_8$ (at. %) obtained at different cooling rates. Compositional analysis of the globules revealed that they consist of two oxides: a nearly continuous matrix of clear tonality (white arrow in Fig. 6d) rich in oxygen ($\text{O}_{60.6}\text{Cu}_{10.9}\text{Zr}_{23.7}\text{Al}_{1.5}\text{Fe}_{2.3}\text{Ni}_{0.9}$) surrounding darker oval areas ($\text{O}_{16.5}\text{Cu}_{38.3}\text{Zr}_{40.7}\text{Al}_{2.7}\text{Ni}_{1.9}$).

The formation of the globular phases (Fig. 6b and 6d) from the surfaces of the existing cubic and dendritic CuZr_2 particles rather than from the amorphous matrix suggests a heterogeneous nucleation process and growth. These are preferential nucleation sites and therefore the effective surface energy is lower, for this reason, it diminishes the free energy barrier and facilitates nucleation leading to lower surface energies [36]. The globular phases are more evolved for the

alloy containing 2 at. % Ni (i.e., 15NNi2) than for the alloy without Ni (i.e., 15NNi0), despite the friction tests were carried out at exactly the same conditions, probably because the T_g for the Ni-containing alloy is about 25°C lower (Table 1). This means that the temperature rise on the sliding surface can more easily reach the T_g for the 15NNi2 sample, resulting in viscous flow. Above the T_g atoms can easily diffuse, with atoms having much larger variety of configurations than below the T_g [37]. This results in higher diffusion of the atoms for the 15NNi2 than for 15NNi0 accounting for the larger growth of the dendrites. The higher tendency for oxidation of the dendrites for 15NNi2 than for 15NNi0 would corroborate this assumption since oxidation in supercooled liquid state conditions (viscous flow above T_g) proceeds faster than under solid state conditions (below T_g).

Along with the cubic and the dendritic particles embedded in the amorphous matrix, there are some finely dispersed phases such as those shown on the inset of Fig. 6a (see arrow). In order to study these phases in detail TEM analysis has been carried out (Fig. 7). For the 1NNi0 sample (Fig. 7a) cubic-like particles and dendrites (see inset) of up to 1 μm size are observed. The EDX results suggest that the composition of the cubic particles and dendrites are $\text{Cu}_{37.5}\text{Zr}_{53.3}\text{Al}_{9.2}$ (Zr/Cu~1.42) and $\text{Cu}_{43.0}\text{Zr}_{50.1}\text{Al}_{6.9}$ (Zr/Cu~1.17) and thus may correspond to CuZr_2 and CuZr respectively. The Selected Area Diffraction Pattern (SADP) for the cubic-like particle (top right pattern) recorded along the zone axis [1 1 0] indicates that the crystalline phase has a tetragonal structure (I_4/mmm , space group 139) which corresponds to CuZr_2 . Additionally, Fig. 7b shows that the sample contains very finely dispersed crystalline particles embedded in a featureless matrix that is amorphous as deduced from the ring of the SADP (inset). Three types of small particles seem to be present according to the morphology and composition: round particles up to 0.1 μm in size (composition: $\text{Cu}_{40.2}\text{Zr}_{52.7}\text{Al}_{7.0}$), flower-like round particles up to 0.2 μm in size (composition: $\text{Cu}_{41.9}\text{Zr}_{52.6}\text{Al}_{5.5}$) and long particles smaller than 0.5 μm (composition: $\text{Cu}_{44.5}\text{Zr}_{51.1}\text{Al}_{4.5}$). All these particles exhibit similar composition with a Zr/Cu ratio of 1.31, 1.26 and 1.15, respectively but with slight different content in Al.

For the 15NNi0 sample, TEM analysis of this composition shows twins in a large crystalline phase (Fig. 7c arrow) of the same morphology to those previously observed in similar alloy systems [17]. The SADP of this twinned phase consists of the superposition of two different diffraction patterns (see inset of Fig. 7c) B2 austenite (bright spots) and B19' martensite (darker spots indexed in red), thus confirming that the striations correspond to twins (austenite transforms into martensite through twinning) [38]. The composition of this phase is $\text{Cu}_{48.8}\text{Zr}_{49.7}\text{Al}_{1.6}$, i.e., Zr/Cu~1, much poorer in Al than the nominal composition and therefore confirms our previous statement that it corresponds to CuZr martensite (i.e., austenite transforms into martensite through twinning) [16]. Additional small particles homogeneously distributed within the amorphous matrix (Fig. 7d) and in larger volume fraction than for 1NNi0 sample can be observed. This is consistent with the higher temperatures attained for 15 N, thus suggesting that the temperatures reached upon friction not only promotes heterogeneous crystallization from the surface of the initially existing particles and dendrites but also crystallization from the matrix. The SADP from the matrix (inset Fig. 7d) shows a

diffuse halo and some spots (marked with red circles), which confirms that the matrix is mostly amorphous but contains also some nanocrystals.

For the 1NNi2 sample, the bright field TEM images (Fig. 7e and 7f) show the presence of crystalline particles of different geometries embedded in an amorphous matrix. The dendrites of Fig. 7e have a composition of $\text{Cu}_{34.3}\text{Zr}_{48.3}\text{Ni}_{10.2}\text{Al}_{7.3}$ (at. %) and thus may correspond to CuZr_2 . Similarly to the analysis of the matrix in the previous cases, different small particles were seen (Fig. 7f): flower-like particles 0.5 μm in size ($\text{Cu}_{36.0}\text{Zr}_{45.3}\text{Ni}_{10.2}\text{Al}_{8.5}$) and round particles less than 0.2 μm in size ($\text{Cu}_{35.9}\text{Zr}_{45.4}\text{Ni}_{10.9}\text{Al}_{7.7}$). The mentioned particles have similar composition but the round particles up of 0.1 μm size are slightly richer in Al. The Zr/Cu ratio (~ 1.26) suggests that both particles may be CuZr_2 crystals. Finally, no great differences in the SADP of the amorphous matrix were detected (inset Fig. 7f) when compared to the 1NNi0 alloy.

TEM images for the 15NNi2 sample are shown in Figs. 7g and 7h. The microstructure consists of different crystalline phases and some of the grains are twinned (see white arrow in Fig. 7g). The corresponding SADP pattern of these grains could not be obtained due to the small grain sizes (less than 50 nm). Nevertheless, this phase could correspond to CuZr martensite. The TEM image obtained from a different area (Fig. 7h) shows oval particles of 0.3 μm in size and grey particles embedded in a matrix. The composition of the oval particles is $\text{Cu}_{61.4}\text{Zr}_{31.9}\text{Ni}_{5.4}\text{Al}_{1.4}$, in contrast to the grey particles and the crystalline phase surrounding them, $\text{Cu}_{46.0}\text{Zr}_{43.6}\text{Ni}_{5.5}\text{Al}_{5.0}$ and $\text{Cu}_{45.8}\text{Zr}_{42.4}\text{Ni}_{6.4}\text{Al}_{5.4}$, respectively. The Zr/Cu ratio of these phases (0.52, 1.05 and 0.93) suggests the presence of CuZr and Cu_8Zr_3 particles. The SADP of the big oval particles taken from the [3 -2 -2] zone axis (upper inset Fig. 7h) corresponds to Cu_8Zr_3 . On the other hand, the SADP of the matrix shows small crystal-like diffraction spots which indicates that the matrix is nanocrystalline (lower inset Fig. 7h).

3.2.3. Estimated contact temperature

The contact temperature rise has been calculated assuming a stationary pin (material 2) and a moving flat steel disk (material 1) using the following equation [20]:

$$\Delta T_{max} = \frac{1.32b\mu pV}{\sqrt{\pi(K_1\sqrt{1.2344+Pe_1}+K_2\sqrt{1.2344+Pe_2})}} \quad (\text{eq. 1})$$

where b , μ , p , V , K and Pe are the contact radius, friction coefficient, normal pressure, sliding velocity, thermal conductivity and the Peclet number respectively. Some of these parameters depend on the elastic constants (E and ν), the density (ρ), the thermal conductivity (K) and the specific heat (C) for the pin samples without Ni, with 1 and 2 at. % Ni and the values have been calculated as a ponderation of the constituent elements constants using the following equation [39-41]:

$$M^{-1} = \sum f_i \cdot M_i^{-1} \text{ (eq. 2)}$$

where M_i and f_i denote any elastic constant and the atomic percentage of the constituent element, respectively. The calculated values for the three alloys and for steel are listed in Table 3. From these values and from the normal pressure, which depends on the load (i.e., 1, 5, 10 and 15 N) and the coefficient of friction, the contact temperature rise has been calculated using eq. 2 and the results are listed on Table 4. The table shows that for most of the loads applied, the estimated temperature increase caused by friction is much lower than the glass transition and crystallization temperatures. However, for the highest load of 15 N the temperature of the Ni-containing pins is around the T_g and therefore the 3600 seconds duration of the wear test (this would be equivalent to an isothermal test) is enough for the material to enter into the supercooled liquid region and result in partial crystallization and oxidation. These oxides act as lubricant thus preventing excessive wear at high loads. Additionally, the CuZr phase work-hardens during the test and, consequently, this helps to further lower the wear rate [42].

These results show that a good strategy for preventing excessive mass loss of metallic glasses with increasing load caused by delamination is to use dopants that decrease the T_g of the alloy close to the friction temperature. This promotes partial surface crystallization and subsequent oxidation thus enhancing the wear resistance and lubrication that can reduce the mass loss.

Partial crystallization is known to enhance the hardness and wear resistance of metallic glasses [2], especially if it undergoes martensitic transformation. Additionally, the surface oxides enhance lubrication of the contact surface and therefore decreases the friction coefficient (see Fig. 3a) thus decreasing the contact surface temperature (eq. 1).

At the same time, addition of Ni as dopant does not have a negative effect on the bulk properties of the material as can be deduced from the similar mass loss value when 1 N load is applied (Fig. 3 and Fig. 4) (i.e., at low load no surface transformation takes place and therefore the results are representative of the bulk material).

This strategy for preventing excessive wear at high loads could be useful for future tribological applications to extend the lifetime of components subjected to wear.

4. Conclusions

Here we propose a new strategy to prevent excessive wear rate of metallic glass composites upon dry sliding at high loads. This consists of doping using an element in adequate concentration to decrease the glass transition temperature (T_g) of the alloy to temperatures close to or slightly below the expected friction temperature. Proper doping promotes partial surface crystallization and oxidation (i.e., lubrication) resulting in a decrease of the wear rate. Suitable doping can also modify the wear resistance when the selected doping element is in the right concentration to promote the martensitic transformation.

Delamination is the main wear mechanism detected for the studied alloys ($\text{Cu}_{45.5}\text{Zr}_{51}\text{Al}_{3.5}$, $\text{Cu}_{44.5}\text{Zr}_{51}\text{Al}_{3.5}\text{Ni}_1$ and $\text{Cu}_{43.5}\text{Zr}_{51}\text{Al}_{3.5}\text{Ni}_2$ at. %) and it is responsible for the progressive mass loss increase with increasing load from 1 to 10 N. At 15 N load, however, the evolution of the mass loss depends on the alloy composition:

- For the Ni-containing alloys the T_g is close to the calculated friction temperature and therefore partial crystallization and oxidation occur. For this reason, the mass loss decreases from about 2.6 to 2.1 mg when the load increases from 10 to 15 N.
- For the alloy without Ni, however, the mass loss at 15 N load increases dramatically to about 3.8 mg because the crystallization is very limited and no oxidation has been detected.

The strategy presented in this work can help to control the wear rate at high loads through proper doping in order to control the glass transition temperature (T_g) of the alloy. Comparing the T_g with the expected calculated friction temperature (ΔT_{\max}) enables to estimate whether the alloy will exhibit massive wear ($\Delta T_{\max} \ll T_g$) or decreased wear ($\Delta T_{\max} \geq T_g$) at a specific load and therefore to tailor the wear performance. Consequently, proper doping is a useful strategy to extend the service life of components subjected to wear under working conditions such as microgears and bearings.

5. Acknowledgements

SG is grateful to the Royal Society for the grant RG2015R2. V.M.V and S.G. acknowledge research support from Northumbria University. Partial financial support from RG2015R2 is acknowledged. J. Medina and P. Pérez would like to acknowledge the expert support of A. García and A. Tomás for assistance with SEM/TEM observations.

6. References

- [1] R.C.Y. Tam, C.H. Shek, Abrasion resistance of Cu-based bulk metallic glasses, *J. Non-Cryst. Alloys* 347 (2004) 268-272.
- [2] A. Inoue, Stabilization of metallic supercooled liquid and bulk amorphous alloys, *Acta Mater.* 48 (2000) 279-306.
- [3] M. Anis, W.M. Rainforth, H.A. Davies, Wear behaviour of rapidly solidified Fe₆₈Cr₁₈Mo₂B₁₂ alloys, *Wear* 172 (1994) 1587-1590.
- [4] J. Eckert, U. Kühn, N. Mattern, A. Reger-Leonhard, M. Heilmaier, Bulk nanostructured Zr-based multiphase alloys with high strength and good ductility, *Scripta Mater.* 44 (2001) 1587-1590.
- [5] C.Y. Tam, C.H. Shek, Abrasive wear of Cu₆₀Zr₃₀Ti₁₀ bulk metallic glass, *Mater. Sci. Eng., A* 384 (2004) 138-142.
- [6] M.L. Rahaman, L.C. Zhang, H.H. Ruan, Effects of environmental temperature and sliding speed on the tribological behaviour of a Ti-based metallic glass, *Intermetallics* 52 (2014) 36-48.
- [7] L. Liu, H. Zhang, C. Shi, Sliding tribological characteristics of a Zr-based bulk metallic glass near the glass transition temperature, *Tribol. Lett.* 33 (2009) 205-210.
- [8] E.D. Tingle, The importance of surface oxide film in the friction and lubrication of metals. Part 1. The dry friction of surfaces freshly exposed to air, *Trans. Faraday Society* 46 (1950) 93-102.
- [9] M. Zhang, D. Yao, X. Wang, L. Deng, Air oxidation of a Zr₅₅Cu₃₀Al₁₀Ni₅ bulk metallic glass at its supercooled liquid state, *Corr. Sci.* 82 (2014) 410-419.
- [10] X.Y. Fu, T. Kasai, M.L. Falk, D.A. Rigney, Sliding behavior of metallic glass: Part I. Experimental investigations, *Wear* 250 (2001) 409-419.
- [11] M.L. Rahaman, L.C. Zhang, H.H. Ruan, Effects of environmental temperature and sliding speed on the tribological behaviour of a Ti-based metallic glass, *Intermetallics* 52 (2014).
- [12] M.L. Rahaman, L. Zhang, On the estimation of interface temperature during contact sliding of bulk metallic glass, *Wear* 320 (2014).
- [13] M.L. Rahaman, L. Zhang, M. Liu, W. Liu, Surface roughness effect on the friction and wear of bulk metallic glasses, *Wear* 332 (2015) 1231-1237.
- [14] M.L. Rahaman, L.C. Zhang, H.H. Ruan, Understanding the friction and wear mechanisms of bulk metallic glass under contact sliding, *Wear* 304 (2013) 43-48.
- [15] S. Hattori, A. Tainaka, Cavitation erosion of Ti-Ni base shape memory alloys, *Wear* 262 (2007) 191-197.
- [16] Y. Wu, D.Q. Zhou, W.L. Song, H. Wang, Z.Y. Zhang, D. Ma, X.L. Wang, Z.P. Lu, Ductilizing bulk metallic glass composite by tailoring stacking fault energy, *Phys. Rev. Lett.* 109 (2012) 245506.
- [17] S. González, P. Pérez, E. Rossinyol, S. Suriñach, M.D. Baró, E. Pellicer, J. Sort, Drastic influence of minor Fe or Co additions on the glass forming ability, martensitic transformations and mechanical properties of shape memory Zr-Cu-Al bulk metallic glass composites, *Sci. Technol. Adv. Mater.* 15 (2016) 035015.
- [18] N. Nishiyama, K. Amiya, A. Inoue, Bulk metallic glasses for industrial products, *Mater. Trans.* 45 (2004) 1245-1250.
- [19] M. Ishida, H. Takeda, N. Nishiyama, K. Kita, Y. Shimizu, Y. Saotome, A. Inoue, Wear resistivity of super-precision microgear made of Ni-based metallic glass, *Mater. Sci. Eng.* 449 (2007).
- [20] H. Wu, I. Baker, Y. Liu, X. Wu, P.R. Munroe, J. Zhang, Tribological studies of a Zr-based bulk metallic glass, *Intermetallics* 35 (2013) 25-32.
- [21] A. Takeuchi, A. Inoue, Classification of Bulk Metallic Glasses by Atomic Size Difference, Heat of Mixing and Period of Constituent Elements and Its Application to Characterization of the Main Alloying Element, *Mater. Trans.* 46 (2005) 2817-2829.
- [22] Z.P. Lu, C.T. Liu, A new glass-forming ability criterion for bulk metallic glasses, *Acta Mater.* 50 (2002) 3501-3512.
- [23] Y. Yokoyama, A. Inoue, Compositional dependence of thermal and mechanical properties of quaternary Zr-Cu-Ni-Al bulk glassy alloys, *Mater. Trans.* 48 (2007) 1282-1287.
- [24] P.J. Blau, Friction and wear transitions of materials: break-in, run-in, wear-in, Noyes Publications, Place, (1989).
- [25] Y. Huang, H. Fan, D. Wang, Y. Sun, F. Liu, J. Shen, J. Sun, J. Mi, The effect of the cooling rate on the wear performance of a ZrCuAlAg bulk metallic glass, *Mater. Des.* 58 (2014) 284-289.
- [26] J. Bhatt, S. Kumar, C. Dong, B.S. Murty, Tribological behaviour of Cu₆₀Zr₃₀Ti₁₀ bulk metallic glass, *Mater. Sci. Eng., A* 458 (2007) 290-294.

- [27] Y. Liu, Z. Yitian, L. Xuekun, Z. Liu, Wear behavior of a Zr-based bulk metallic glass and its composites, *J. Alloy. Compd.* 503 (2010) 138-144.
- [28] N.P. Suh, *Tribophysics*, Prentice-Hall, Place, (1986).
- [29] H. Yang, Y. Liu, T. Zhang, H. Wang, B. Tang, J. Qiao, Dry sliding tribological properties of a dendrite-reinforced Zr-based bulk metallic glass matrix composite, *J. Mater. Sci. Technol.* 30 (2014) 576-583.
- [30] W.U. Hong, I. Baker, L.I.U. Yong, X.L. Wu, Dry sliding tribological behavior of Zr-based bulk metallic glass, *Trans. Nonferrous Met. Soc. China* 22 (2012) 585-589.
- [31] X.F. Wu, G.A. Zhang, F.F. Wu, Wear behaviour of Zr-based in situ bulk metallic glass matrix composites, *Bull. Mater. Sci.* 39 (2016) 703-709.
- [32] G. Effenberg, S. Ilyenko, *Light metal ternary systems: Phase diagrams, crystallographic and thermodynamic data Vol. 11A2*, Materials Science International Team MSIT, Place, (2007).
- [33] H. Bo, J. Wang, S. Jin, H.Y. Qi, X.L. Yuan, L.B. Liu, Z.P. Jin, Thermodynamic analysis of the al-cu-zr bulk metallic glass system, *Intermetallics* 18 (2010) 2322-2327.
- [34] X. Bai, J.H. Li, Y.Y. Cui, Y. Dai, N. Ding, B.X. Liu, Formation and structure of cu-zr-al ternary metallic glasses investigated by ion beam mixing and calculation, *J. Alloys Compd.* 522 (2012) 35-38.
- [35] J.L. Cheng, G. Chen, Glass formation of Zr-Cu-Ni-Al bulk metallic glasses correlated with $L \rightarrow Zr_2Cu + ZrCu$ pseudo binary eutectic reaction, *J. Alloys Compd.* 577 (2013) 451-455.
- [36] U. Köster, Surface crystallization of metallic glasses, *Mater. Sci. Eng.* 97 (1988) 233-239.
- [37] U. Geyer, S. Schneider, W.L. Johnson, Y. Qiu, T.A. Tombrello, M.P. Macht, Atomic diffusion in the supercooled liquid and glassy states of the $Zr_{41.2}Ti_{13.8}Cu_{12.5}Ni_{10}Be_{22.5}$ alloy, *Phys. Rev. Lett.* 75 (1995) 2364-2367.
- [38] M. Arciniegas, J. Casals, J.M. Manero, J. Pena, F. J. Gil, Study of hardness and wear behaviour of NiTi shape memory alloys, *J. Alloys Compd.* 460 (2008) 213-219.
- [39] W.H. Wang, Roles of minor additions in formation and properties of bulk metallic glasses, *Prog. Mater. Sci.* 52 (2007) 540-596.
- [40] S. Li, X.K. Xi, Y.X. Wei, Q. Luo, Y.T. Wang, M.B. Tang, B. Zhang, Z.F. Zhao, R.J. Wang, M.X. Pan, D.Q. Zhao, W.H. Wang, Formation and properties of new heavy rare-earth-based bulk metallic glasses, *Sci. Technol. Adv. Mater.* 6 (2005) 823-827.
- [41] Y.X. Wei, B. Zhang, R.J. Wang, M.X. Pan, D.Q. Zhao, W.H. Wang, Erbium-and cerium-based bulk metallic glasses, *Scripta Mater.* 54 (2006) 599-602.
- [42] J. Singh, A.T. Alpas, Dry sliding wear mechanisms in a $Ti_{50}Ni_{47}Fe_3$ intermetallic alloy, *Wear* 181 (1995) 302-311.
- [43] G.W.C. Kaye, T.H. Laby, *Tables of physical and chemical constants*, Longman, Place, (1993).
- [44] A. M. James, M.P. Lord, *Macmillan's Chemical and Physical Data*, Macmillan, Place, (1992).
- [45] C.Y. Ho, R.W. Powell, P.E. Liley, Thermal conductivity of the elements: a comprehensive review, *J. Phys. Chem. Ref. Data* 3 (1974) 1-588.
- [46] M. Baucchio, *ASM Metals Reference Book*, ASM International, Place, (1993).
- [47] P.D. Harvey, *Engineering Properties of Steels*, American Society for Metals, Place, (1982).
- [48] M. Yamasaki, S. Kagao, Y. Kawamura, Thermal diffusivity and conductivity of Zr 55 Al 10 Ni 5 Cu 30 bulk metallic glass, *Scripta Mater.* 53 (2005) 63-67.

Figure Captions

Fig. 1. XRD scans for (a) $\text{Cu}_{45.5}\text{Zr}_{51}\text{Al}_{3.5}$, (b) $\text{Cu}_{44.5}\text{Zr}_{51}\text{Al}_{3.5}\text{Ni}_1$ and (c) $\text{Cu}_{43.5}\text{Zr}_{51}\text{Al}_{3.5}\text{Ni}_2$ at. % alloys.

Fig. 2. DSC curves for (a) $\text{Cu}_{45.5}\text{Zr}_{51}\text{Al}_{3.5}$, (b) $\text{Cu}_{44.5}\text{Zr}_{51}\text{Al}_{3.5}\text{Ni}_1$ and (c) $\text{Cu}_{43.5}\text{Zr}_{51}\text{Al}_{3.5}\text{Ni}_2$ heated at 20 K/min up to 773 K. The inset highlights the enlarged section of DSC curves around the T_g .

Fig. 3. (a) Friction coefficient and (b) mass loss of the $\text{Cu}_{45.5}\text{Zr}_{51}\text{Al}_{3.5}$, $\text{Cu}_{44.5}\text{Zr}_{51}\text{Al}_{3.5}\text{Ni}_1$, and $\text{Cu}_{43.5}\text{Zr}_{51}\text{Al}_{3.5}\text{Ni}_2$ alloys for loads applied for 1 hour from 1 to 15 N. Inset: friction coefficients as a function of time.

Fig. 4. Secondary electron SEM images of the samples after the test for the different compositions and loads. Insets: magnified images showing the presence of small (red circles) and larger (arrows) cracks.

Fig. 5. Backscattered SEM images and EDX scans for the selected areas of $\text{Cu}_{45.5}\text{Zr}_{51}\text{Al}_{3.5}$ sample tested at (a) 1 N and (b) 15 N load.

Fig. 6. Secondary electron SEM images for $\text{Cu}_{45.5}\text{Zr}_{51}\text{Al}_{3.5}$ (at. %): (a) 1NNi0 and (b) 15NNi0. For $\text{Cu}_{43.5}\text{Zr}_{51}\text{Al}_{3.5}\text{Ni}_2$ (at. %): (c) 1NNi2 and (d) 15NNi2 after pin-on-disc tests.

Fig. 7. TEM images for $\text{Cu}_{45.5}\text{Zr}_{51}\text{Al}_{3.5}$ (at. %): (a, b) 1NNi0 and (c, d) 15NNi0. For $\text{Cu}_{43.5}\text{Zr}_{51}\text{Al}_{3.5}\text{Ni}_2$: (e, f) 1NNi2 and (g, h) 15NNi2 after pin-on-disc tests.

Table 1. DSC data for $\text{Cu}_{45.5}\text{Zr}_{51}\text{Al}_{3.5}$, $\text{Cu}_{44.5}\text{Zr}_{51}\text{Al}_{3.5}\text{Ni}_1$ and $\text{Cu}_{43.5}\text{Zr}_{51}\text{Al}_{3.5}\text{Ni}_2$ alloys.

Table 2. Code for the different conditions of composition and load.

Table 3. Mechanical properties for the Temperature estimation calculated from the properties of the elements [43-45] and properties of EN31 steel [46, 47].

Table 4. Contact temperature rise (Kelvin) for all the different compositions and loads.

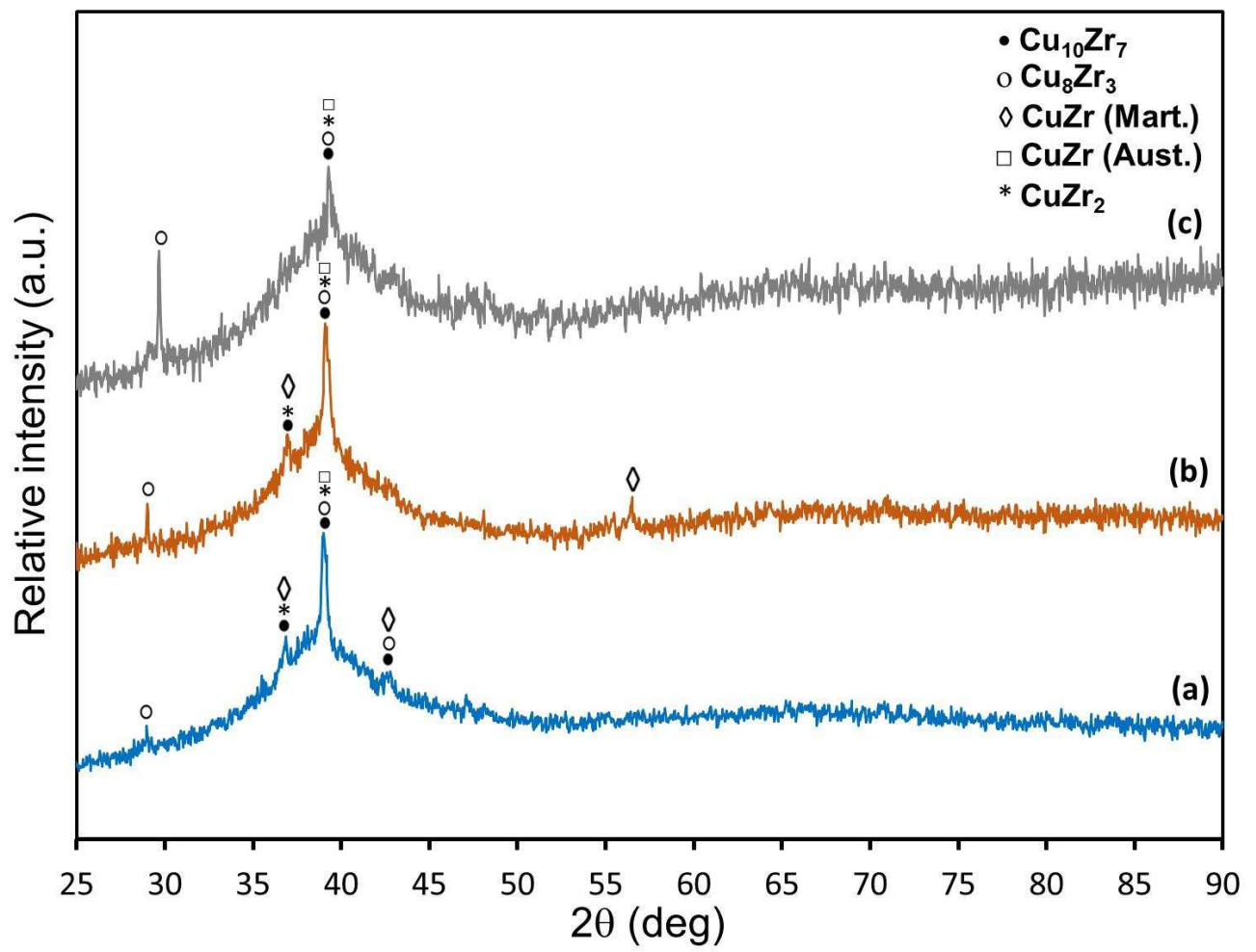


Figure 1

ACCEPTED

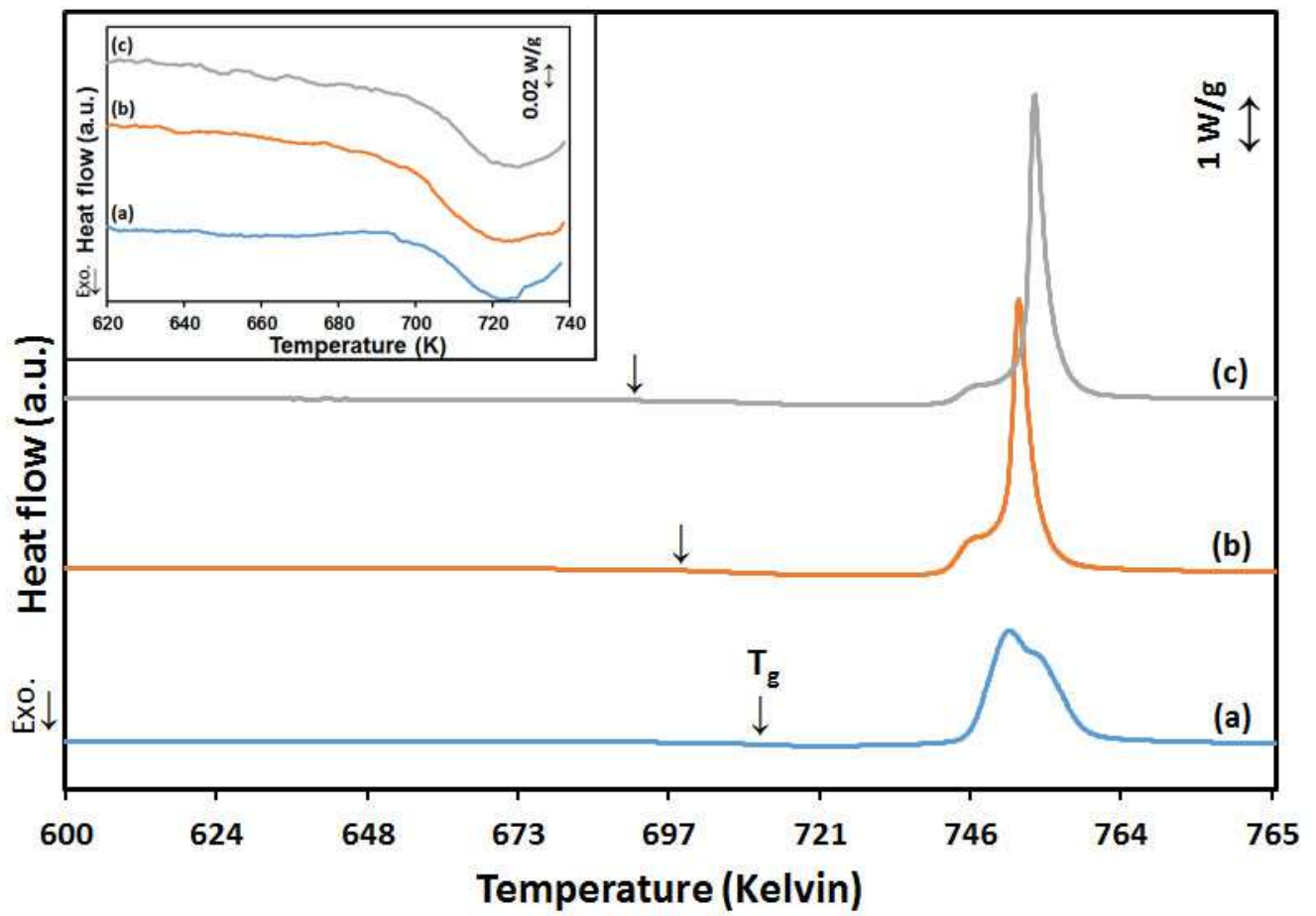


Figure 2

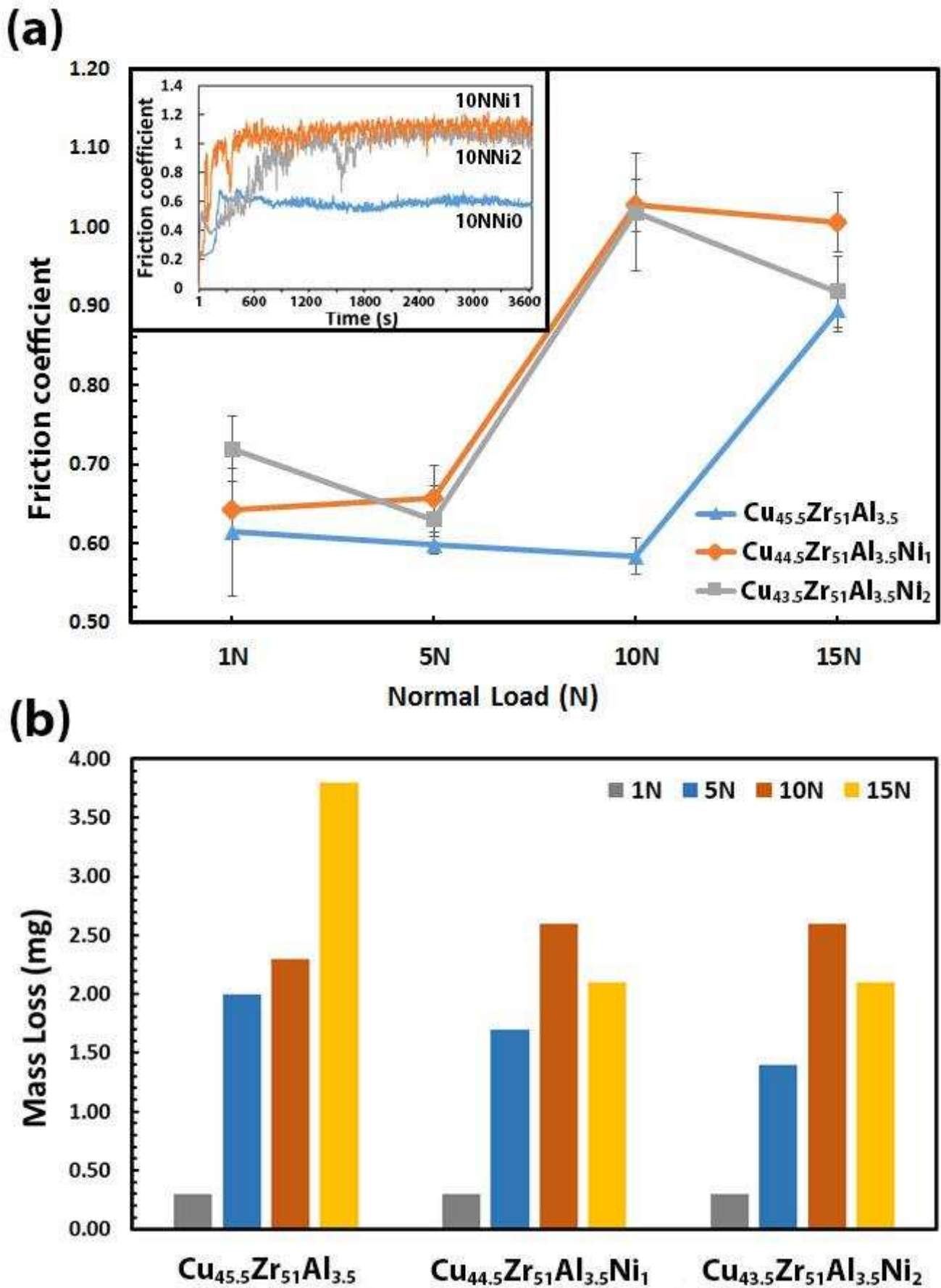


Figure 3

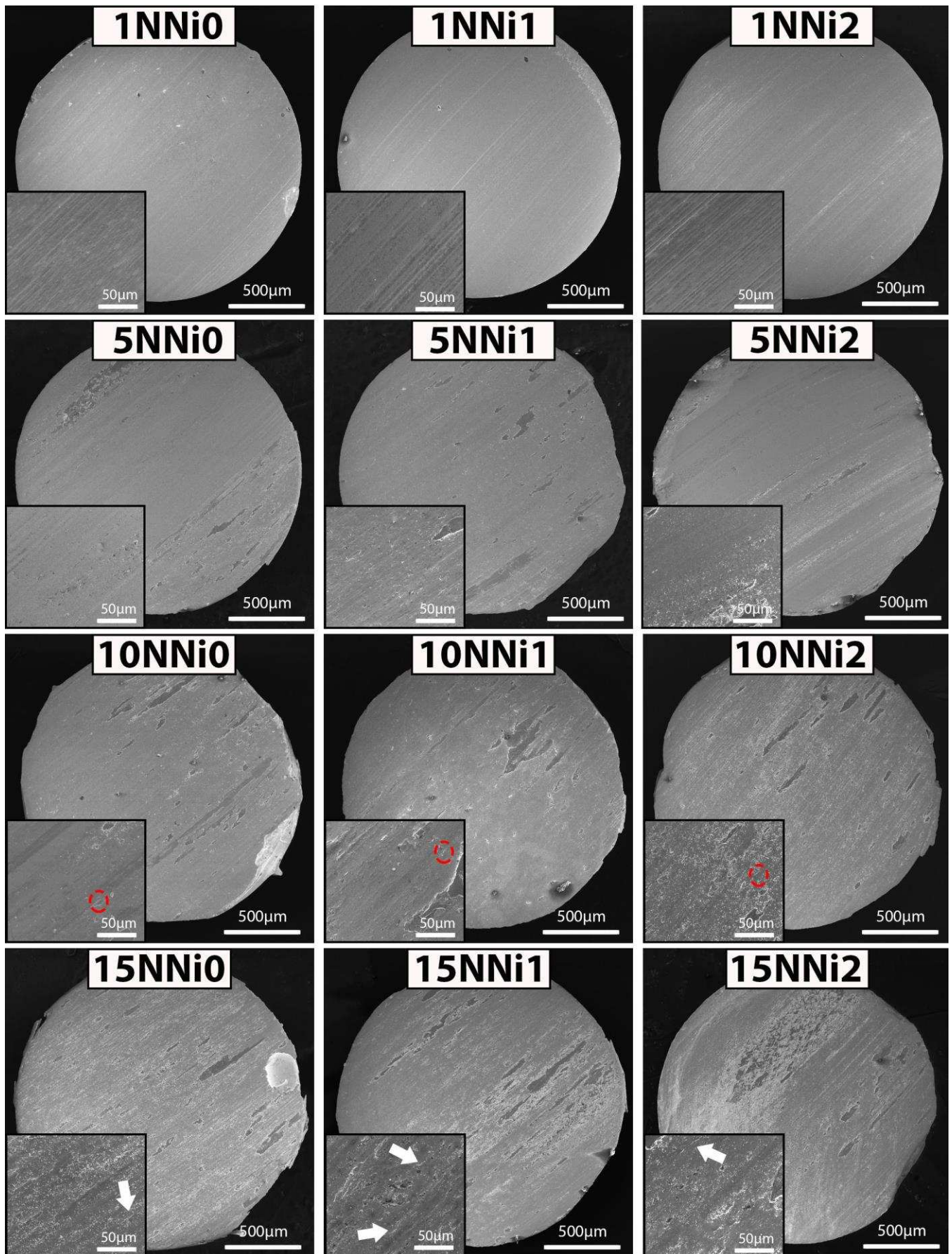


Figure 4

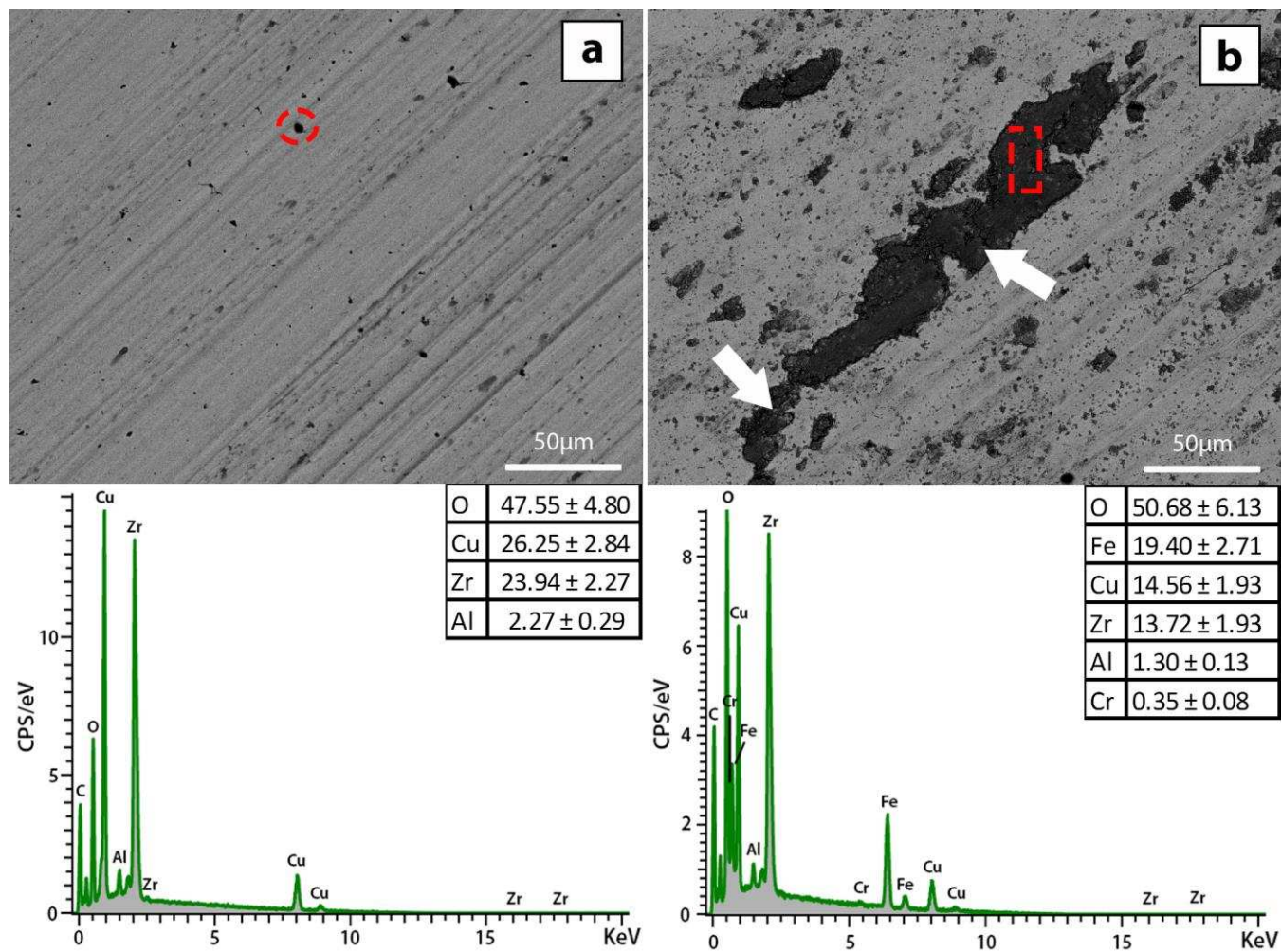


Figure 5

ACCEPTED MANUSCRIPT

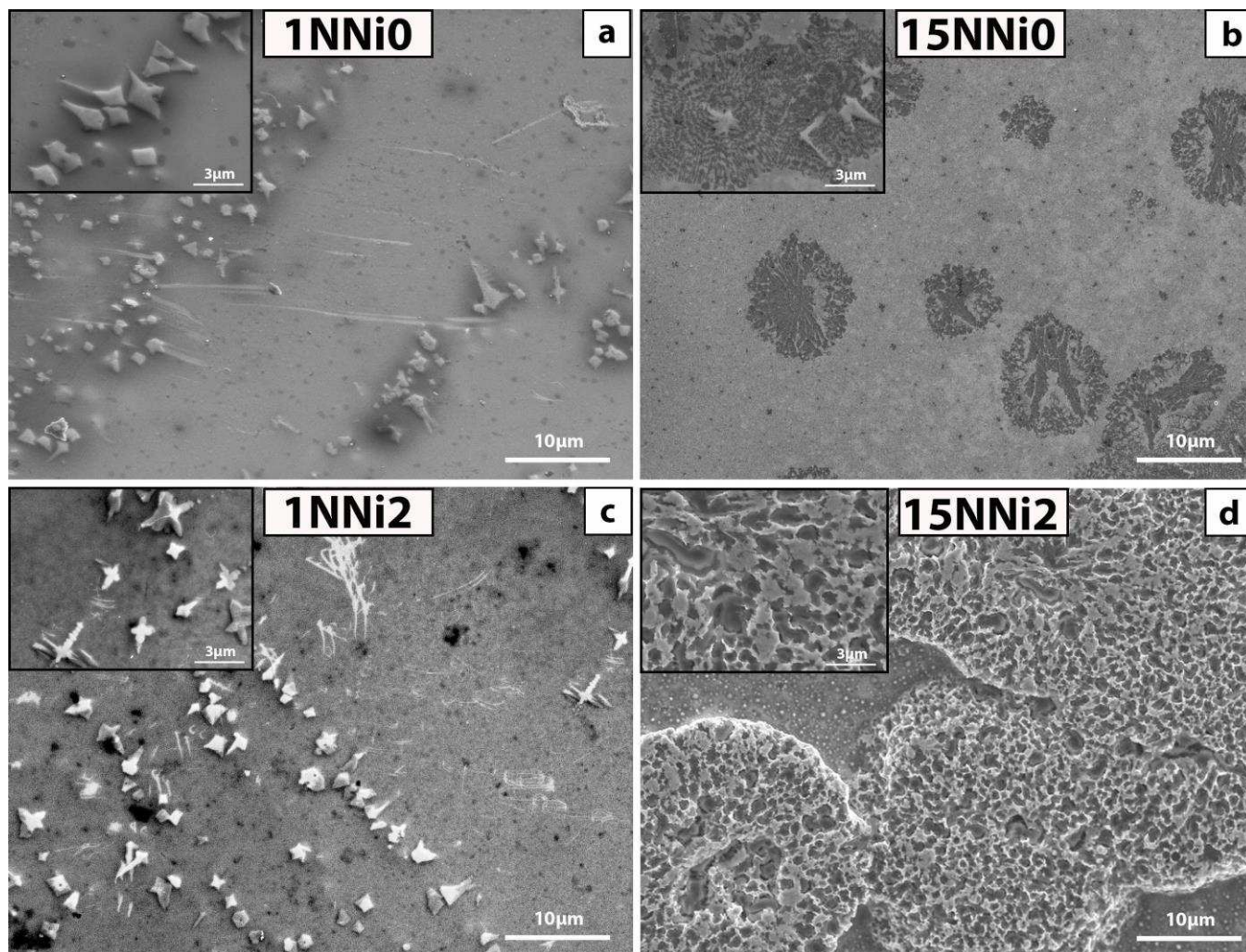


Figure 6

ACCEPTED

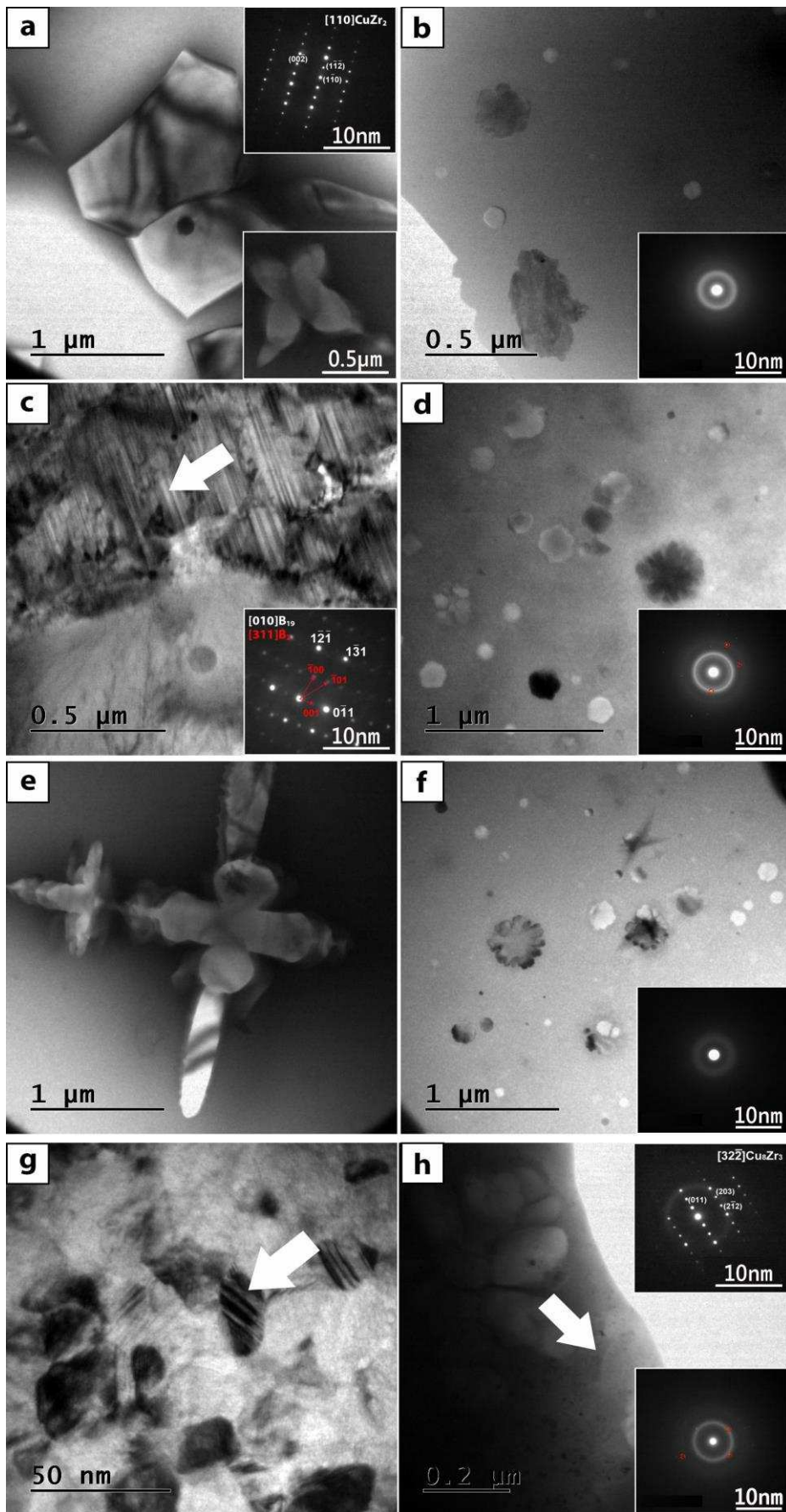


Figure 7

Table 1. DSC data for $\text{Cu}_{45.5}\text{Zr}_{51}\text{Al}_{3.5}$, $\text{Cu}_{44.5}\text{Zr}_{51}\text{Al}_{3.5}\text{Ni}_1$ and $\text{Cu}_{43.5}\text{Zr}_{51}\text{Al}_{3.5}\text{Ni}_2$ alloys.

Composition (at. %)	T_g (K)	T_x (K)	$\Delta T = T_x - T_g$ (K)	H (J/g)
$\text{Cu}_{45.5}\text{Zr}_{51}\text{Al}_{3.5}$	710.84	744.87	34.03	47.05
$\text{Cu}_{44.5}\text{Zr}_{51}\text{Al}_{3.5}\text{Ni}_1$	697.77	740.57	42.80	49.08
$\text{Cu}_{43.5}\text{Zr}_{51}\text{Al}_{3.5}\text{Ni}_2$	685.39	740.06	54.66	42.54

ACCEPTED MANUSCRIPT

Table 2. Code for the different conditions of composition and load.

Composition (at. %)			
Load	$\text{Cu}_{45.5}\text{Zr}_{51}\text{Al}_{3.5}$	$\text{Cu}_{44.5}\text{Zr}_{51}\text{Al}_{3.5}\text{Ni}_1$	$\text{Cu}_{43.5}\text{Zr}_{51}\text{Al}_{3.5}\text{Ni}_2$
1N	1NNi0	1NNi1	1NNi2
5N	5NNi0	5NNi1	5NNi2
10N	10NNi0	10NNi1	10NNi2
15N	15NNi0	15NNi1	15NNi2

ACCEPTED MANUSCRIPT

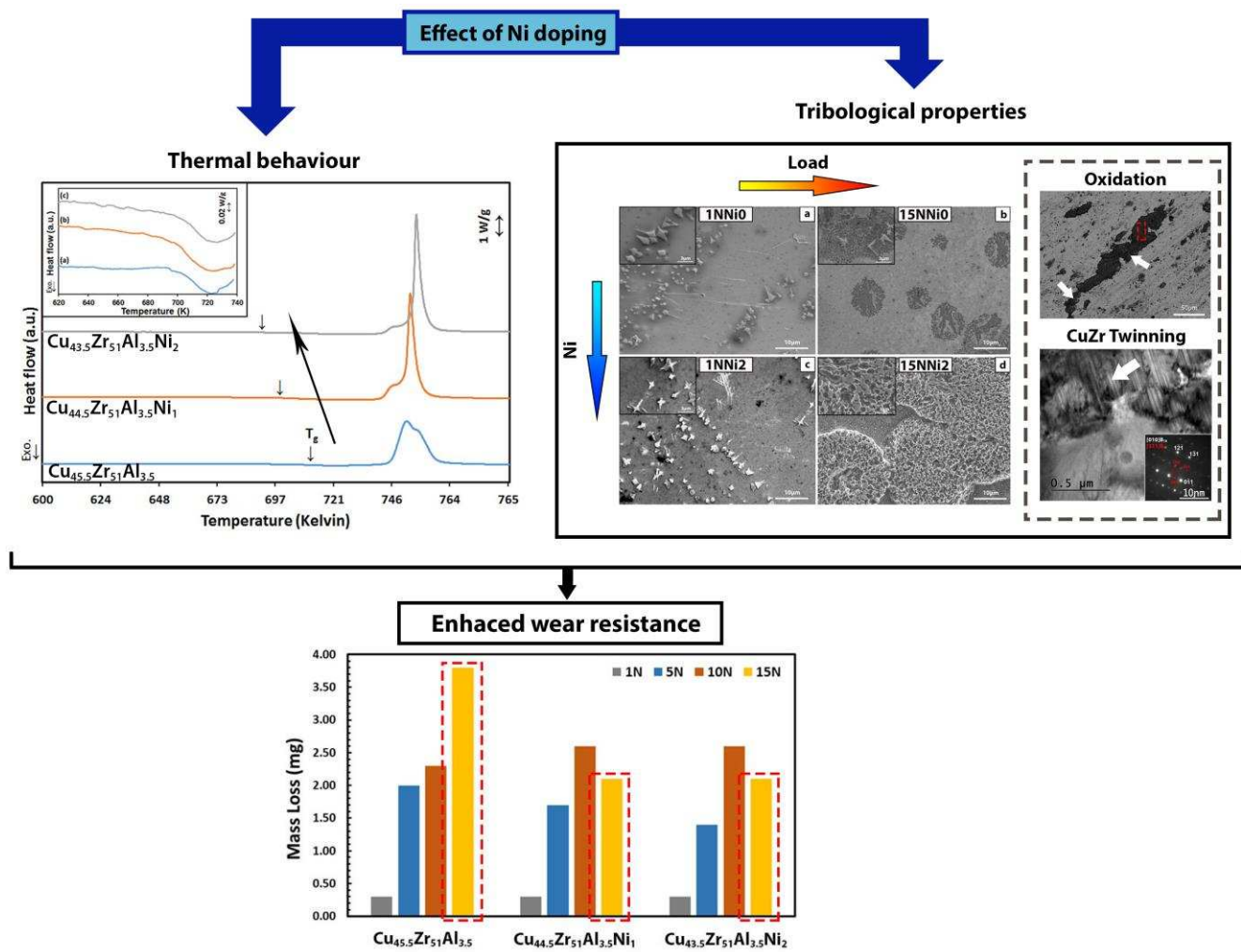
Table 3. Mechanical properties for the Temperature estimation calculated from the properties of the elements [41-43] and properties of EN31 steel [44,45].

	Cu	Zr	Al	Ni	Steel	$\text{Cu}_{45.5}\text{Zr}_{51}\text{Al}_{3.5}$	$\text{Cu}_{44.5}\text{Zr}_{51}\text{Al}_{3.5}\text{Ni}_1$	$\text{Cu}_{43.5}\text{Zr}_{51}\text{Al}_{3.5}\text{Ni}_2$
E (GPa)	130.00	68.00	70.00	200.00	210.00	86.96	87.16	87.37
ρ (Kg/m ³)	8920.00	6511.00	2700.00	8908.00	7800.00	7027.36	7027.29	7027.21
ν	0.34	0.34	0.35	0.31	0.30	0.34	0.34	0.34
K (W/mK)	401.00	22.70	237.00	90.90	46.60	5.03 [46]	5.03 [46]	5.03 [46]
C (Nm/KgK)	384.40	278.00	904.00	445.00	475.00	327.13	327.51	327.89

Table 4. Contact temperature rise (Kelvin) for all the different compositions and loads.

	$\text{Cu}_{45.5}\text{Zr}_{51}\text{Al}_{3.5}$	$\text{Cu}_{44.5}\text{Zr}_{51}\text{Al}_{3.5}\text{Ni}_1$	$\text{Cu}_{43.5}\text{Zr}_{51}\text{Al}_{3.5}\text{Ni}_2$
1 N	342.66	344.89	351.15
5 N	423.37	436.24	430.42
10 N	486.29	633.35	630.68
15 N	670.22	717.78	680.78

ACCEPTED MANUSCRIPT



Graphical abstract

Highlights

- Small Ni addition decreases the glass transition temperature of the Cu-Zr-Al alloy.
- The mass loss during the wear test increases with increasing load from 1 to 10 N.
- The friction temperature can be close to the glass transition temperature.
- Partial crystallization and oxidation results in wear resistance increase.

ACCEPTED MANUSCRIPT